Environmental Science & Technology

pubs.acs.org/est

Article

Microfluidic Screening to Study Acid Mine Drainage

Die Yang, Rong Fan, Christopher Greet, and Craig Priest*

Cite This: *Environ. Sci. Technol.* 2020, 54, 14000−14006

Read Online

ACCESS | Metrics & More | Article Recommendations | Supporting Information

ABSTRACT: Acid mine drainage (AMD) is the most significant environmental pollution problem associated with the mining industry. Case-specific testing is widely applied and established in the mining and consulting businesses for AMD prediction, and any improvements in its efficiency, while reducing its environmental impact, are of utmost societal importance. In this study, we develop a microfluidic screening method as a useful tool in the prediction and, potentially, prevention and remediation of AMD. The new approach offers key advantages including high throughput screening of reaction conditions, better spatiotemporal control over the process, and ability to conduct field-based measurements, which will account for specific interactions between mineral ores and their environment. Reagent and sample consumptions are greatly reduced to mL and mg levels, compared with those in conventional bulk-scale screening. Parallel (multichip) screening of ferric ion concentration gradients (0−40 mM) and temperature (23−75 °C) is demonstrated here, showing that the dissolution rate of pyrite significantly changes with the pH, temperature, and the ferric ion concentration, consistent with previous bulk-scale studies. To verify the robustness of the method, a mine waste rock was also tested in the microchip with natural waters. This study demonstrates the application of microfluidic screening to the challenging issue of AMD and, more generally, forecasting and optimization of mineral leaching in industry.

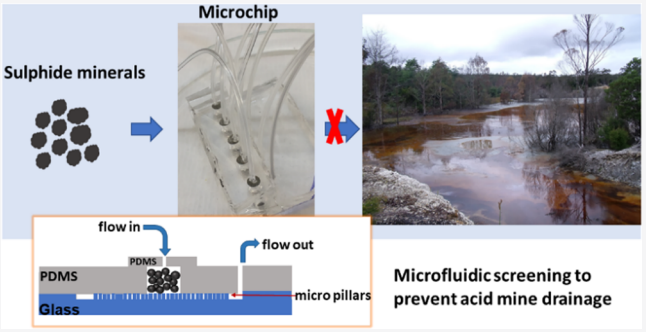

KEYWORDS: *microfluidics, screening, acid mine drainage, leaching, mineral processing*

INTRODUCTION

Acid mine drainage (AMD) occurs when sulfide minerals are exposed to oxidizing conditions, e.g., water and oxygen. This occurs naturally where sulfide minerals exist in water-saturated zones, but this process can be considerably accelerated by the production of broken waste rock and tailings through mining operations. Sulfide-bearing mining waste can produce large volumes of contaminated effluents with elevated acidity and often contains toxic amounts of dissolved heavy metals (such as Fe, Cu, Mn, Zn and Pb).[1,2] Due to its severe environmental impact on soil, water resources, and aquatic environments,[3,4] AMD has become one of the greatest environmental issues facing the mining industry. The prediction and control of AMD therefore poses key elements in the strategy to control pollution from mining operations.[5] Although the fundamental chemistry of AMD formation has been extensively examined, the resulting profiles of waste rock and tailings are highly dependent on several factors including geological setting, mineralogy, presence of microorganisms, and other environmental variables such as temperature, oxygen, and water.[6] These factors are highly variable for any given mine site, and therefore, rapid kinetic testing of waste rock and tailings under actual field conditions at mine sites using portable devices are highly desirable for the evaluation and prediction of their long-term AMD behaviors and potential remediation pathways.

Current practice of AMD assessment of sulfide-bearing mining wastes primarily involves long-term acid generation/alkalinity definition under batch, column, and drum leach conditions in order to evaluate the acid generation, sulfate release, and metal release rates based on specific sulfide reaction pathways. A number of procedures have been developed to determine the acid forming characteristics of mine waste materials and long-term AMD prediction and control.[7] More broadly, toxicity characteristic leaching procedure (TCLP) is an accepted standard method for characterizing solid waste, including leached heavy metals and volatile organics in environmental remediation and rehabilitation. However, these tests for the evaluation and prediction of environmental pollutants, particularly AMD, are time-consuming and plagued with an insufficient spatiotemporal control associated with the large volumes of the reactors used.[5] Moreover, accurate control of essential physio-chemical variables of these large-scale experiments, such as temperature, are unrealistic over the longer term. Screening measurements

Received: May 23, 2020
Revised: October 1, 2020
Accepted: October 7, 2020
Published: October 21, 2020

https://dx.doi.org/10.1021/acs.est.0c02901
Environ. Sci. Technol. 2020, 54, 14000−14006

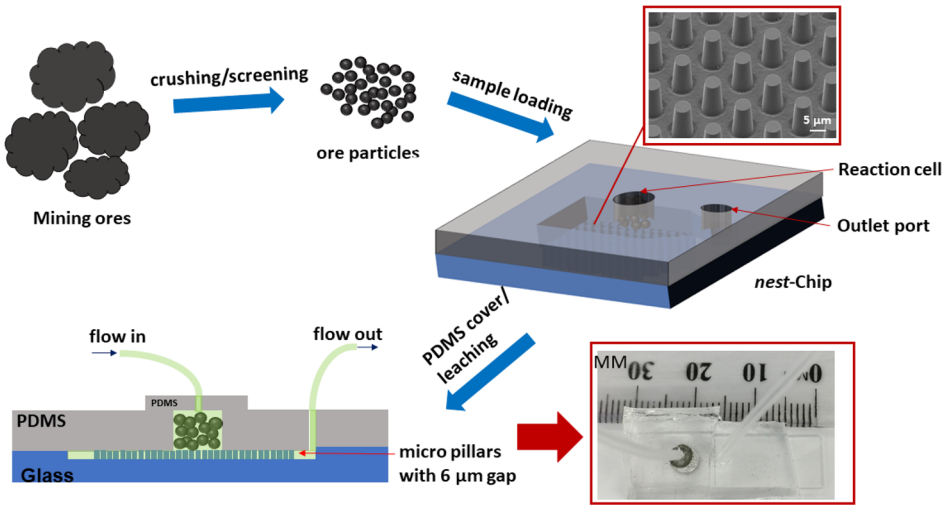

Figure 1. Schematic illustration of the workflow for a single nest in the leach screening platform. Crushed and screened ore particles can be quickly and easily loaded into the nest and contacted with various aqueous conditions to investigate AMD formation. Inset: An SEM image of 6 μm pillars (upper right) and an image of the experimental setup with inlet and outlet tubing (lower right, single nest shown).

that cover the necessary physical or chemical properties require a relatively large quantity of samples and reagents.

The application of lab-on-a-chip or microfluidic technologies to geological studies is an emerging field, where the unique benefits afforded by system miniaturization offer new opportunities such as high-throughput screening of experimental variables, increasing flexibility in running multiple screening parameters and evaluating the interplay between the components. Despite the immaturity of this field, studies of geological phenomena using microfluidic platforms have been extremely diverse and are ever expanding, as highlighted by recent articles discussing the exploitation of microfluidics to oil recovery,[8−11] CO_2 capture/storage,[12,13] and release of K^+ from soil minerals.[14,15] Our studies have demonstrated the potential benefits of using microfluidics in mineral leaching processes for investigating reactions pathways and mechanisms, correlative surface analysis, and high throughput screening of chemical or physical parameters that influence the leaching rate and process.

To date, only a few examples of microfluidic testing using real rock samples have been reported.[12,16,17] These studies generally employed two-dimensional models, where a PDMS microchannel is sealed against a flat sample (e.g., thin gold film,[18] calcite,[12] chalcopyrite[16]) and allows detailed studies of dissolution, leaching, and liquid displacement processes. However, natural formations (such as minerals) are typically rough and inhomogeneous, which significantly complicates dissolution, adsorption, leaching, and other physio-chemical processes related geological phenomena. To this end, we developed a robust microfluidic method for screening geological phenomena that occur at the solid/liquid interface of particle samples (as received). Evaluation of mineral dissolution/leaching for a range of reaction conditions was carried out using real rock samples with species diversity. We chose to screen for AMD under typical environmental (field) conditions; however, the method can also be applied to optimization of industrial leach processes at mineral processing plants.

Pyrite (FeS_2), the most abundant sulfide mineral in the earth's crust, is a primary contributor to AMD and release of sulfide bearing mining wastes. It was therefore chosen for this study. The rate of pyrite oxidation and the resulting acid production are dependent on various environmental factors that are dynamic and vary substantially between regions. Here, ferric ion concentration, pH, and temperature (which are the common factors affecting the oxidation of pyrite) were examined by loading individual "nests" in a chip (see Figure 1). For each experiment, only 50 mg of the sample is required. Reagent consumption is approximately 3 mL for screening up to 6 h reaction time. Five parallel experiments were demonstrated here, although the method allows for greater parallelization as required. Surface characterization of the solid residue was carried out by X-ray photoelectron spectroscopy (XPS) to correlate the surface chemistry of the reaction residue with the leaching behavior observed by solution analysis. A real waste rock sample was also tested in the microchip with natural waters to verify the robustness of the developed methodology.

MATERIALS AND METHODS

Materials. Pyrite ore sample (FeS_2) was supplied by Geo Discoveries (NSW, Australia). The phase purity of the pyrite ore was confirmed by quantitative X-ray diffraction and chemical analyses, and detailed characterizations have been described elsewhere.[19] The ore was then crushed, ground, and screened to a particle size range of 38−75 μm with particle surface area measured at 0.35 $m^2 \cdot g^{-1}$.[19] Mine waste rock was collected from a closed copper−zinc mine in central Newfoundland, Canada. The elemental composition of the waste rock was measured using $HCl/HNO_3/HF$ analytical microwave assisted digestion (EPA Method 3052) followed by inductively coupled plasma atomic emission spectroscopy (ICP-AES) on a subsample ground to particle size of <75 μm. Chemical composition of the sample gives 4.3 wt % Al, 30.4 wt % Si, 4.1 wt % Fe, 69 ppm of Cr, 1204 ppm Mn, 1335 ppm of Cu, 2437 ppm Zn, and 118 ppm Pb. Quantitative XRD mineralogy suggests that the waste rock contains 56 wt % quartz, 20 wt % muscovite, 10 wt % clinochlore (chlorite), 4 wt % pyrite, 3 wt % siderite with minor gypsum, sphalerite, chalcopyrite. The sample was air-dried, ground, and passed through a 75 μm sieve before microchip leaching. The natural water sample was collected from local watersheds (Mawson

https://dx.doi.org/10.1021/acs.est.0c02901
Environ. Sci. Technol. 2020, 54, 14000−14006

Lakes, South Australia), filtered through 0.45 μm-pore-size membrane filters, and then stored at 0−4 °C for further use.

KOH (1 M, AR, 85%) and HCl (37%) were used to adjust the pH of the solution. $FeCl_3.6H_2O$ (AR) was used for the preparation of ferric ion concentrations. KCl (0.1 M) was used as the background electrolyte to ensure the solution ionic strengths were approximately constant throughout the experiments. All chemicals were purchased from Chem-Supply, Australia. Milli-Q water (18 MΩ·cm resistivity) was used to prepare all solutions.

Design of *Nest*-Chip. A schematic representation of the ore-on-a-chip system is shown in Figure 1. Crushed and screened ore particles were transferred to open reaction cells ("nests") within the microfluidic chip and contacted with various aqueous solutions under controlled flow, temperature, and pH conditions to investigate AMD formation. The nests are formed in an upper polymer layer and bonded to a bottom substrate layer containing an array of micropillars. The micropillars serve as a support structure that is impermeable to the ore particles but allows the fluid (i.e., leaching reagent in this study) to pass through for collection. Glass materials are applied in this study for optical observation, but other materials may be suitable. The ore particles are held as a packed bed above the micropillars in the reaction cell. In this study, 6 μm diameter circular pillars arranged in a square lattice with 12 μm lattice period was used to ensure that the pillar gap is smaller than the size of the ore particles (38−75 μm). The top polymer layer includes a reaction cell, which is sealed by plastic cover/lid after loading ore particles, and inlet and outlet ports. PDMS is used for this proof-of-concept study for its straightforward and inexpensive fabrication and chemical compatibility.

This design of microfluidic chip allows quick and easy loading of ore samples as received. The leached analyte was collected at the outlet for ICP analysis. The reaction rate, pH, temperature, and other solution properties can be monitored during the process. Parallel testing of several samples can be carried out using a nest array, and high-throughput studies are possible with further parallelization (the five chip nest does not represent a physical limit). The cell cover/lid, positioned on the top of the reaction cell, can be easily detached after reaction finish to allow for surface characterization of the solid residue after leaching.

Fabrication of Microfluidic Chips. The microfluidic device for this study is assembled by sealing a layer of polydimethylsiloxane (PDMS) layer (thickness ∼8 mm) on a pillar cuvette (with 6 μm pillar separation and 10 μm pillar height)[20,21] through plasma bonding, with loading cell and outlet port precored in the PDMS. During bonding, care was taken to align the loading cell and outlet port regions within the pillar cuvette. The fabrication of the PDMS layer was carried out according to a procedure described elsewhere.[22] A mass ratio of 10:1 of Sylgard 184 silicone elastomer base and curing agent was mixed thoroughly and poured onto a hydrophobized silicon wafer-based container. The PDMS was cured at 60 °C for 4 h and then peeled off from the silicon master. After which, the loading cell and outlet ports were cored using 4 mm and 1.5 mm biopsy punches, respectively. The cross-section of the assembled chip is illustrated in Figure 1. After loading the ore samples, the open reaction cell was sealed with a thin layer of PDMS which allows the introduction of flow via TYGON tubing or optical inspection of the reaction cell, as required.

Leach Experiment. For each leach experiment, the flow was driven by peristatic pump (Gilson, Minipuls®3) through capillary tubing (0.5 mm inner and 1.58 mm outer diameter) into the reaction cell at 0.65 ± 0.05 mL h^{-1}. The leach solutions were collected at the outlet through capillary tubing in a glass vial over a period of 1 h for each sample. A schematic of the overall experimental setup is given in Figure 1. For screening, five leach experiments at various ferric concentrations (0, 5, 10, 20, and 40 mM, respectively) were conducted in parallel under controlled temperature that was controlled using a transparent electrical heater below the microchip. The large area heater ensured that the temperature was uniform across the entire nest of chips. The flow for parallel experiments were driven by multiple channels on a single peristatic pump to ensure the same flow rate in each test. Note that ferric ion concentrations and temperatures were chosen to reflect actual field conditions at mine sites for the evaluation of the performance of the developed microchip for AMD study. Leaching of real mine waste rock samples followed the same procedure as that of pyrite samples. All leaching samples were collected at the outlet and stored in sealed vials at 0−4 °C before being analyzed by inductively coupled plasma mass spectrometry (ICP-MS) (Agilent 8800). The average leach rate ($mM \cdot m^{-2} \cdot s^{-1}$) during the collection period (1 h per measurement) was determined from the ion concentration in the collected leach solution and sample surface area. Screening experiments were repeated three times with similar results, showing an experimental error within 6%.

Surface Analysis. After leach or acid wash, the ore samples were rinsed with milli-Q water to remove any residue leachate. The PDMS was then removed, and the wet samples were quickly transferred into a small plastic vial with rinsing water and stored in the freezer for cold stage (−134 °C) XPS analysis. XPS spectra were collected using a Kratos AXIS Ultra DLD spectrometer. The X-ray was a monochromatic aluminum X-ray running at 225 W with a characteristic energy of 1486.6 eV. The area of analysis (Iris aperture) was a 0.3 mm × 0.7 mm slot; the analysis depth was approximately 15 nm into the surface of the sample. The analysis vacuum was 4×10^{-8} Torr. The electron takeoff angle was normal to the sample surface. Spectra were interpreted using the software package CasaXPS.

RESULTS AND DISCUSSION

Pyrite Dissolution Kinetics and Surface Pretreatment. The flow chemistry applied in the microfluidic devices enables the examination of reaction dynamics, particularly in the early stages of the leaching experiments, which are difficult to access using conventional methods. Figure 2 shows the evolution of the leachate chemistry for both dissolved Fe and S in pyrite as a function of time (up to 6 h). A rapid decline in both S and Fe in the leachate was observed for the untreated pyrite sample compared to the acid washed sample in the first 2 h, suggesting that acid washing has removed the more reactive surface layer that contains both Fe and S species. The leachate chemistry (for S and Fe, respectively) was quite stable and very similar at the later stage of leaching for both untreated and treated (acid washed) samples. This may be attributed to the dissolution of fresh pyrite exposed during the course of leaching. The Fe/S ratio (0.41−0.46) observed at later stage in the leachate for both pyritic samples is slightly below the stoichiometric dissolution of pyrite (0.5). Generally, the result shows that that the acid wash (pretreatment) has no impact on the leach

https://dx.doi.org/10.1021/acs.est.0c02901
Environ. Sci. Technol. 2020, 54, 14000−14006

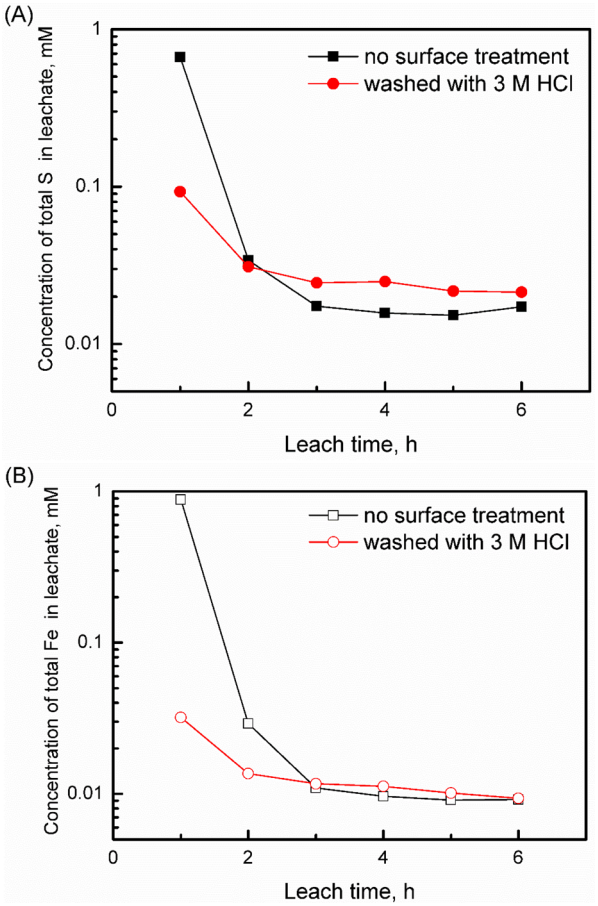

Figure 2. Comparison of S (A) and Fe (B) release rate from pyrite as a function of time without surface treatment and washed with 3 M HCl. These experiments were conducted at room temperature, 0.6–0.7 mL h^{-1} flow rate, pH 2, and 0.1 M KCl.

behavior of intrinsic pyrite mineral. Therefore, for further investigation of AMD formation under various conditions, acid wash was used as standard sample treatment before running experiments. Further details about the surface chemistry of outer layer of pyrite before and after leach will be discussed in Surface Characterization section. No surface passivation was observed under the conditions examined during the leach time.

Effect of pH. The effect of pH on the dissolution rate per unit surface area of pyrite ($mM.m^{-2}.s^{-1}$) was examined in the pH range of 2–10. The leach rates of each element at different pH were calculated from the measured solution total S or Fe concentration divided by sample's total surface area (determined from the mass and specific surface area of the sample) and collection time for each measurement (1 h). The average value of the leach rate at steady state (after initial removal of oxidation layer) was then plotted against pH (error bars represent the standard deviation of the obtained leach rates), as shown in Figure 3.

Figure 3 shows that the pH has a significant but very different impact on the leach (release) rate of S and Fe from pyrite. The higher the pH, the higher the concentration of sulfur compounds in solution. However, the concentration of Fe detected in solution was decreased as the pH increased. When the pH was higher than 7, only trace amounts of Fe were detected in solution. The Fe/S ratio calculated from the total Fe and S species detected in the solutions declined from 0.46 to 0.008 as the pH increased from 2 to 10, i.e., the pyrite

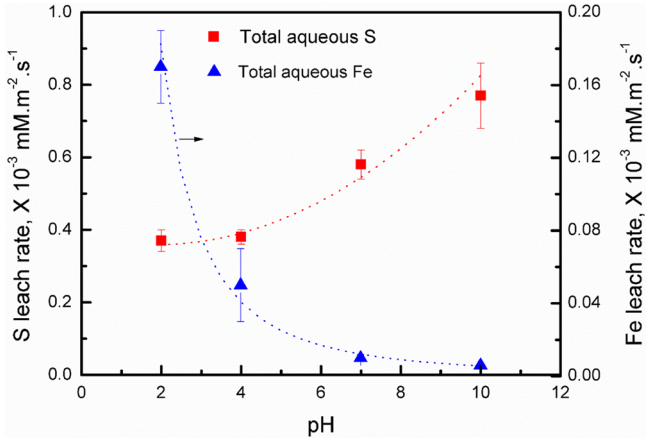

Figure 3. Aqueous Fe and S released from pyrite as a function of pH at room temperature with ionic strength of 0.1 M KCl and 0.6–0.7 mL h^{-1} flow rate.

surface did not exhibit the expected stoichiometric dissolution (Fe/S = 0.5) at high pH. This is most probably due to the formation of Fe precipitate as iron (hydro)oxides at pyrite surface, as suggested in previous studies.[23,24] As the pH increased further, more iron (hydro)oxides grew at the pyrite surface; however, this did not prevent further pyrite oxidation because sulfur species are still released to the solution at increasing rate as shown in Figure 3. Similar leach behavior was observed in a previous study.[23] Note that the reaction rate obtained is around 4 orders of magnitude higher than that of previously reported values at similar reaction conditions,[19] probably due to the continuous flow of fresh leaching solution and continuous removal of byproducts from the pyrite sample.

The log rate of pyrite dissolution ($mol{\cdot}m^{-2}{\cdot}s^{-1}$) plotted against pH (Supporting Information Figure S1) showed a reaction order for pH of 0.04 (with a R square factor of 0.96) in the range of pH 2–10, which is lower than reported values, which vary widely between 0.11 to 0.5.[25,26] The small reaction order of the present study for H^+ indicates that pH has a smaller effect on observed rate compared to batch-scale experiments, due to the continuous removal of iron precipitates (formed at higher pH) in the microfluidic flow system avoiding possible surface passivation. Note that S concentration detected in the leachate was applied for the calculation of pyrite dissolution rate instead of Fe, due to the precipitate of iron species at pyrite surface during the leaching at higher pH.

Combinatorial Screening (Temperature, Ferric Ion Concentration, and Time). The microfluidic platform is attractive for the screening of multiple variables of same or different natures within a single platform because it benefits from the minimization of the reaction system. In this study, ferric ion concentration and temperature were chosen as screening parameters for the study of AMD. Each nest was exposed to different leach conditions, enabling rapid parameter screening (results shown in Figure 4).

Figure 4 shows the screening results for varied ferric ion concentrations (0, 5, 10, 20, and 40 mM ferric ion concentration in the fresh leach solution) for three different temperatures (23, 50, and 75 °C). The average pyrite dissolution rates were determined at steady state (observed between 3 to 6 h) based on the sulfur concentration measured in the leachate. The relationship between the leach rate and the

https://dx.doi.org/10.1021/acs.est.0c02901
Environ. Sci. Technol. 2020, 54, 14000–14006

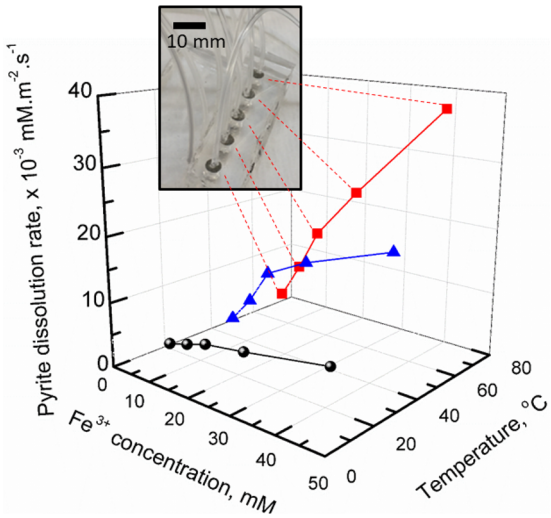

Figure 4. 3D graph of the dissolution rate of pyrite as a function of temperature and ferric ion concentration with ionic strength of 0.1 M KCl in the solution, 0.6−0.7 mL h^{-1} flow rate, and pH 2. Inset: Image of a screening chip with five samples nests for parallel screening of five Fe^{3+} concentrations for a single temperature (e.g., red symbols).

two variables (temperature and Fe^{3+} concentration) is clearly seen in Figure 4. An increase in either variable increases the leach rate, consistent with previous studies[26,27] but uses several orders of magnitude less sample, reagent, and time. Surface passivation was not observed under the examined conditions, which is likely due to the continuous flow of fresh leach solution in this study. It might be possible to study surface passivation by recirculating the leach solution; however, this was not tested in the present study. On the basis of the above results, we calculated the reaction order of pyrite dissolution rate on Fe^{3+} concentration as 0.72 ± 0.06 (shown in Figure S2), which is close to the values reported in the literature.[26] The Arrhenius plot shows the apparent activation energy of the pyrite oxidation reaction by ferric ion solution is around 30.6 ± 0.7 kJ mol^{-1}, consistent with previously reported values ranging between 33 and 63 kJ mol^{-1}.[28,29]

Surface Analysis by XPS. Due to the formation of iron precipitate on the pyrite surface during leaching, analysis of the sulfur signal may be more useful than that of iron. S (2p) XPS spectra of the pyrite samples treated at different conditions, untreated, acid washed (3 M HCl), and leached for 6 h at pH 2, are shown in Figure S4 (Supporting Information). For all pyrite samples, the characteristic peak located at 162 eV in the S $2p_{3/2}$ spectra agrees with the expected value for pyritic S_2^{2-}.[23] A small S^{2-} peak at 161 eV was also found on all samples. Signals detected in the range of 164−165 eV suggested the presence of elemental S and S_n^{2-} at the surface of all pyrite samples. On untreated samples, there was a peak at 168 eV, attributed to the presence of sulfate species on the surface. This peak intensity was significantly decreased after the acid wash, suggesting sulfate species were removed from the surface during washing. After leaching for 6 h, the peak at 168 eV is barely observed indicating a complete dissolution of sulfates from the surface. No traces of sulphites were found in the 166−167 eV range. These results are in good agreement with the analysis of the leachate solutions collected.

Testing of Mine Waste Rock with Natural Water. To verify the robustness of the microchip for the investigation of AMD, the leaching of real waste rock sample was tested on the chip with natural water. It was observed that under the conditions examined (i.e., room temperature, flow rate of ∼0.7 mL/h, and natural water which has a pH of 5.6), there was no obvious change of the water content within the time examined (6 h). However, a decrease in pH of the water to pH 2 significantly increased the dissolution of the ore particles. As shown in Figure 5, there were significant changes for several

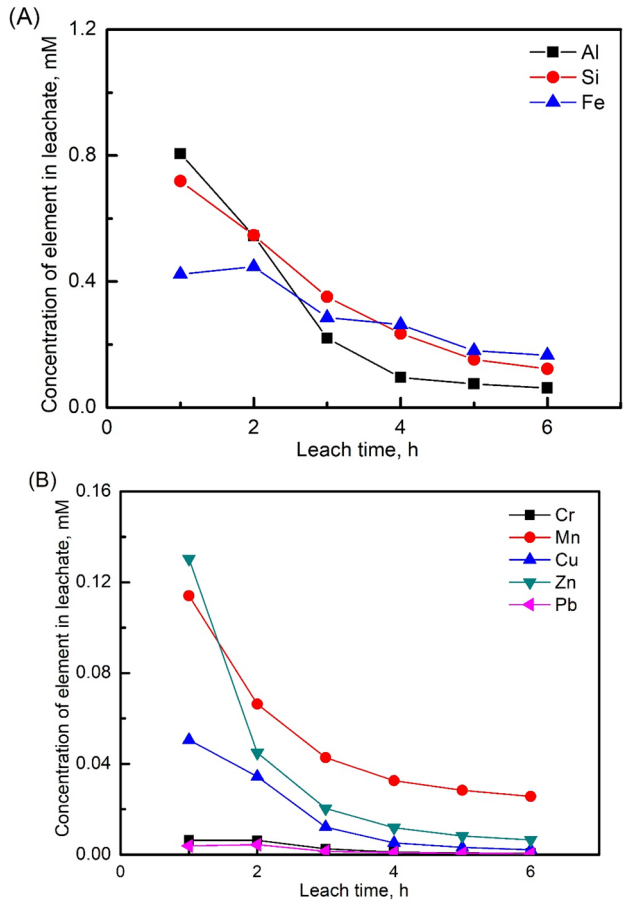

Figure 5. Major elements released into the solution as a function of time during the leach of mine waste rock with natural water. The experiment was conducted at room temperature, ∼0.7 mL h^{-1} flow rate, and pH 2.

elements including Al, Si, Fe, Cr, Mn, Cu, Zn, and Pb in the water that passed through the microchip. Note that a small amount of each element was detected in the feedwater but has been subtracted from the measured concentration in the collected samples to ensure that the reported values represent leached elements only. The evolution of the leachate chemistry was similar as that of pyrite, with a rapid decline of the dissolution rate of metals in the first 2−3 h which then remained stable at the late stage of leaching.

Implications. Microfluidic screening of geological phenomena such as leaching offers a rapid approach to investigating natural processes that are environmentally or commercially important. The complex parameter space encountered in these reaction systems demands high throughput multiparameter screening, using minimal sample, reagent, and time. The microfluidic approach used here meets these demands and is shown to report meaningful time-resolved results for various reaction conditions. The mineral samples can be directly loaded into the device, without the need for flat, large areas

https://dx.doi.org/10.1021/acs.est.0c02901
Environ. Sci. Technol. 2020, 54, 14000−14006

(e.g., polished or embedded in resin). Samples could be obtained directly from mine sites and, in many cases, on site screening would be possible. Low-cost testing could precede field trials, which are typically expensive and time-consuming. In addition, the proposed screening method could be used to study a wide range of solid−liquid interactions in flow (adsorption, dissolution, and other surface chemistry phenomena) across many different fields of application, including outside of AMD and mineral processing.

■ ASSOCIATED CONTENT

Supporting Information

The Supporting Information is available free of charge at https://pubs.acs.org/doi/10.1021/acs.est.0c02901.

The log rate of pyrite dissolution plotted against pH; linear regression analysis of rate data for the aqueous oxidation of pyrite by ferric ion at different temperatures; Arrhenius plot for the oxidation reaction of pyrite at different ferric ion concentrations and temperatures; fitted S (2p) XPS spectra of the pyrite samples treated at different conditions (PDF)

■ AUTHOR INFORMATION

Corresponding Author

Craig Priest − *Future Industries Institute and UniSA STEM, University of South Australia, Mawson Lakes, SA 5095, Australia;* orcid.org/0000-0002-8861-2161; Email: Craig.Priest@unisa.edu.au

Authors

Die Yang − *Future Industries Institute, University of South Australia, Mawson Lakes, SA 5095, Australia*

Rong Fan − *CSIRO Mineral Resources, Clayton South, VIC 3169, Australia*

Christopher Greet − *Magotteaux Australia PTY Ltd, Wingfield, SA 5013, Australia*

Complete contact information is available at: https://pubs.acs.org/10.1021/acs.est.0c02901

Author Contributions

C.P. and C.G. developed the concept. D.Y., R.F., and C.P. designed the experiments. D.Y. conducted the experiments. All authors interpreted the results, prepared the manuscript, and gave approval to the final version of the manuscript.

Notes

The authors declare the following competing financial interest(s): Dr Christopher Greet is Manager, Metallurgy Minerals Processing Research at Magotteaux, and is collaborating with the University of South Australia on commercialization of research.

■ ACKNOWLEDGMENTS

The authors acknowledge the financial support of the Australian Government Department of Industry, Innovation and Science, through the Australia-China Fund award of the Australia-China Joint Research Centre in In Line Chemical and Mineral Sensing for Sustainable Mineral Processing (JRCAF-55), and Magotteaux Australia Pty Ltd for providing in-kind support and scientific advice. The authors also thank Chris Bassell for XPS data collection and Dr Gujie Qian for XPS data analysis. This work was performed in part at the South Australian node of the Australian National Fabrication Facility (ANFF-SA) and Microscopy Australia (MA) facilities under the National Collaborative Research Infrastructure Strategy to provide fabrication and microscopy facilities for Australia's researchers.

■ REFERENCES

(1) Egiebor, N. O.; Oni, B. Acid rock drainage formation and treatment: a review. *Asia-Pac. J. Chem. Eng.* **2007**, *2* (1), 47−62.

(2) Dold, B. Evolution of Acid Mine Drainage Formation in Sulphidic Mine Tailings. *Minerals* **2014**, *4* (3), 621−641.

(3) Sheoran, A. S.; Sheoran, V. Heavy metal removal mechanism of acid mine drainage in wetlands: A critical review. *Miner. Eng.* **2006**, *19* (2), 105−116.

(4) Hogsden, K. L.; Harding, J. S. Consequences of acid mine drainage for the structure and function of benthic stream communities: a review. *Freshwater Science* **2012**, *31* (1), 108−120.

(5) Dold, B. Acid rock drainage prediction: A critical review. *J. Geochem. Explor.* **2017**, *172*, 120−132.

(6) Simate, G. S.; Ndlovu, S. Acid mine drainage: Challenges and opportunities. *J. Environ. Chem. Eng.* **2014**, *2* (3), 1785−1803.

(7) Smart, R. S. C.; Skinner, W.; Levay, G.; Gerson, A.; Thomas, J.; Sobieraj, H.; Schumann, R.; Weisener, C. G.; Weber, P.; Miller, S. *ARD Test Handbook*; AMIRA International Limited Melbourne, 2002.

(8) Gunda, N. S.; Bera, B.; Karadimitriou, N. K.; Mitra, S. K.; Hassanizadeh, S. M. Reservoir-on-a-chip (ROC): a new paradigm in reservoir engineering. *Lab Chip* **2011**, *11* (22), 3785−92.

(9) de Haas, T. W.; Fadaei, H.; Guerrero, U.; Sinton, D. Steam-on-a-chip for oil recovery: the role of alkaline additives in steam assisted gravity drainage. *Lab Chip* **2013**, *13* (19), 3832−9.

(10) Conn, C. A.; Ma, K.; Hirasaki, G. J.; Biswal, S. L. Visualizing oil displacement with foam in a microfluidic device with permeability contrast. *Lab Chip* **2014**, *14* (20), 3968−77.

(11) Lifton, V. A. Microfluidics: an enabling screening technology for enhanced oil recovery (EOR). *Lab Chip* **2016**, *16* (10), 1777−96.

(12) Song, W.; de Haas, T. W.; Fadaei, H.; Sinton, D. Chip-off-the-old-rock: the study of reservoir-relevant geological processes with real-rock micromodels. *Lab Chip* **2014**, *14* (22), 4382−90.

(13) Sharbatian, A.; Abedini, A.; Qi, Z.; Sinton, D. Full Characterization of CO2-Oil Properties On-Chip: Solubility, Diffusivity, Extraction Pressure, Miscibility, and Contact Angle. *Anal. Chem.* **2018**, *90* (4), 2461−2467.

(14) Ciceri, D.; Allanore, A. Microfluidic Leaching of Soil Minerals: Release of K+ from K Feldspar. *PLoS One* **2015**, *10* (10), No. e0139979.

(15) Stanley, C. E.; Grossmann, G.; i Solvas, X. C.; deMello, A. J. Soil-on-a-Chip: microfluidic platforms for environmental organismal studies. *Lab Chip* **2016**, *16* (2), 228−41.

(16) Yang, D.; Kirke, M.; Fan, R.; Priest, C. Investigation of Chalcopyrite Leaching using an Ore-on-a-Chip. *Anal. Chem.* **2019**, *91* (2), 1557−1562.

(17) Gerold, C. T.; Krummel, A. T.; Henry, C. S. Microfluidic devices containing thin rock sections for oil recovery studies. *Microfluid. Nanofluid.* **2018**, *22* (7), 76.

(18) Yang, D.; Priest, C. Microfluidic Platform for High-Throughput Screening of Leach Chemistry. *Anal. Chem.* **2018**, *90* (14), 8517−8522.

(19) Fan, R.; Short, M. D.; Zeng, S. J.; Qian, G.; Li, J.; Schumann, R. C.; Kawashima, N.; Smart, R. S. C.; Gerson, A. R. The Formation of Silicate-Stabilized Passivating Layers on Pyrite for Reduced Acid Rock Drainage. *Environ. Sci. Technol.* **2017**, *51* (19), 11317−11325.

(20) Holzner, G.; Kriel, F. H.; Priest, C. Pillar Cuvettes: Capillary-Filled, Microliter Quartz Cuvettes with Microscale Path Lengths for Optical Spectroscopy. *Anal. Chem.* **2015**, *87* (9), 4757−4764.

(21) Kriel, F. H.; Priest, C. Influence of Sample Volume and Solvent Evaporation on Absorbance Spectroscopy in a Microfluidic "Pillar-Cuvette. *Anal. Sci.* **2016**, *32* (1), 103−8.

(22) Kotova, S.; Follink, B.; Del Castillo, L.; Priest, C. Leaching gold by reactive flow of ammonium thiosulfate solution in high aspect ratio

channels: Rate, passivation, and profile. *Hydrometallurgy* **2017**, *169*, 207−212.
(23) Bonnissel-Gissinger, P.; Alnot, M.; Ehrhardt, J.-J.; Behra, P. Surface Oxidation of Pyrite as a Function of pH. *Environ. Sci. Technol.* **1998**, *32* (19), 2839−2845.
(24) Huminicki, D. M. C.; Rimstidt, J. D. Iron oxyhydroxide coating of pyrite for acid mine drainage control. *Appl. Geochem.* **2009**, *24* (9), 1626−1634.
(25) Williamson, M. A.; Rimstidt, J. D. The kinetics and electrochemical rate-determining step of aqueous pyrite oxidation. *Geochim. Cosmochim. Acta* **1994**, *58* (24), 5443−5454.
(26) Wang, H.; Dowd, P. A.; Xu, C. A reaction rate model for pyrite oxidation considering the influence of water content and temperature. *Miner. Eng.* **2019**, *134*, 345−355.
(27) Wiersma, C. L.; Rimstidt, J. D. Rates of reaction of pyrite and marcasite with ferric iron at pH 2. *Geochim. Cosmochim. Acta* **1984**, *48* (1), 85−92.
(28) Janzen, M. P.; Nicholson, R. V.; Scharer, J. M. Pyrrhotite reaction kinetics: reaction rates for oxidation by oxygen, ferric iron, and for nonoxidative dissolution. *Geochim. Cosmochim. Acta* **2000**, *64* (9), 1511−1522.
(29) Long, H.; Dixon, D. G. Pressure oxidation of pyrite in sulfuric acid media: a kinetic study. *Hydrometallurgy* **2004**, *73* (3−4), 335−349.

https://dx.doi.org/10.1021/acs.est.0c02901
Environ. Sci. Technol. 2020, 54, 14000−14006